Inorganic Chemistry

pubs.acs.org/IC Article

Flux Growth of an Intermetallic with Interstitial Fluorides via Decomposition of a Fluorocarbon

James T. Larson and Susan E. Latturner*



Cite This: Inorg. Chem. 2023, 62, 1508-1512

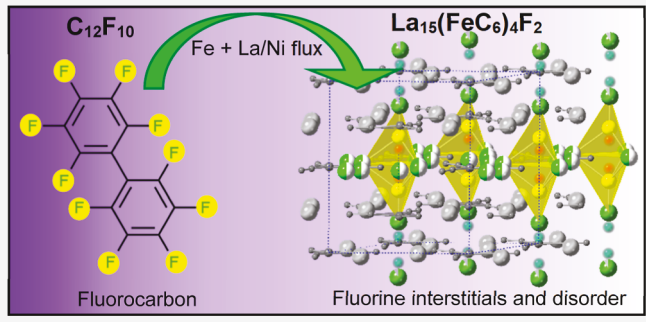


ACCESS I

Metrics & More

Article Recommendations

ABSTRACT: La₁₅(FeC₆)₄F₂ was grown as large crystals by reacting iron in a La/Ni eutectic flux in the presence of decafluorobiphenyl ($C_{12}F_{10}$) which acts as both a carbon and fluoride source. This mild fluorinating technique enables the isolation of an intermetallic product containing fluoride interstitials, as opposed to forming ionic metal fluorides. The compound adopts a structure in the hexagonal crystal system with space group $P\bar{6}$ which features FeC₆ units composed of a central iron atom coordinated by three ethylenide units in a trigonal planar configuration. The structure is related to the previously reported La₁₅(FeC₆)₄H, but with fluoride fully occupying the interstitial hydride positions, which induces partial



occupancies and site splitting disorder in the adjacent layers of lanthanide ions. No supercell formation is observed.

■ INTRODUCTION

Metal flux synthesis offers unique opportunities for the discovery of new materials. Unlike traditional solid-state methods such as the "ceramic method" and arc melting, metal flux synthesis enables reactions to take place at lower temperatures, which increase the likelihood of obtaining kinetically favorable products. Additionally, metal flux synthesis is a solution-based method, providing a good environment for crystal growth with the products often being suitable for single-crystal X-ray diffraction (SC-XRD). The use of rare-earth based flux has been shown to be an excellent synthesis route for new rare earth intermetallics, producing, for example, $Pr_{26}Fe_{19}C_{29}$, $Pr_{21}Fe_{16}Te_6B_{30}$, $Ce_{33}Fe_{13}B_{18}C_{34}$, $La_{15}(FeC_6)_4H$, and $Ce_4B_2C_2H_{2.42}$.

Rare earth containing intermetallics can often incorporate hydrogen on interstitial sites; this is observed in hydrogen storage intermetallics such as LaNi₅H₆, formed when LaNi₅ is exposed to hydrogen gas. ^{9,10} The presence of interstitial hydrides can easily be missed because hydrogen is usually not observable using the most common method of structural analysis, X-ray diffraction. Neutron diffraction is necessary to detect the location and occupancy of hydride sites. Corbett et al. demonstrated that several compounds reported as binary intermetallics actually contain hydride interstitials; for example, they found that members of the β -Yb₅Sb₃ structure type actually contain a hydride site. ^{11–13} Recently, several intermetallic compounds with hydrogen interstitials have been grown by using anthracene as a carbon and hydrogen source (Ce₄B₂C₂H_{2,42} and La₁₅(FeC₆)₄H); incorporation of hydrogen was confirmed by neutron diffraction studies. ^{7,8} To

avoid the necessity for neutron diffraction experiments at a national laboratory, we are exploring the incorporation of fluoride interstitials, which should be detectable using standard X-ray diffraction equipment.

In this work, we observe the formation of $La_{15}(FeC_6)_4F_2$ from the reaction of decafluorobiphenyl ($C_{12}F_{10}$) with iron in La/Ni flux. This reaction yielded large single crystals that were suitable for SC-XRD. This compound is structurally related to $La_{15}(FeC_6)_4H$ reported by Engstrand et al. with fluorine substituting into the hydride site. The siting and occupancy of the fluorine were clearly observable in the SC-XRD data. Unlike in the hydride structure, the presence of fluoride induces disorder (site splitting and partial occupancy) in neighboring lanthanide sites. The success of this reaction indicates that this is a promising route for the substitution of fluorine into complex rare earth metal hydrides.

EXPERIMENTAL PROCEDURE

Warning: pressure may be generated in the reaction ampule when the organic compound decomposes at high temperature. Small amounts of $C_{12}F_{10}$ should be used so that the pressure of gaseous decomposition products (such as F_2) does not exceed 4 atm at maximum temperature. Suitable personal protective equipment

Received: October 14, 2022 Published: January 12, 2023





(gloves and face shields) were used when removing the ampules from the furnace, and they were wrapped in an aluminum foil barrier before breaking them open in a fume hood.

Synthesis. Pellets of 88:12 wt % La/Ni eutectic (mp 530 °C) were prepared to use as the flux to grow $La_{15}(FeC_6)_4F_2$ single crystals. La pieces (BTC 99.9%) and Ni slugs (BTC 99.99% 3.145 × 6.55 mm) were melted together in an arc melter under argon. The pellets were flipped over and remelted several times to ensure homogeneous mixing. After cooling, the pellets were then broken apart using wire cutters to make smaller pieces to fit inside the alumina crucibles used for reactions.

The other reactants are iron powder (Macron 100 mesh, stored under nitrogen) and decafluorobiphenyl (C₁₂F₁₀, TCI 98.0%), used in a ratio of 1:0.2 mmol. Iron was placed inside an alumina crucible, followed by approximately 1.5 g of the La/Ni flux. Decafluorobiphenyl was placed at the bottom of a silica sleeve, and the alumina crucible containing the other reactants was placed on top. Two crucial steps must be noted. It was found to be necessary to use iron powder that has not oxidized; traces of FeOOH or other oxides and hydroxides can lead to increased pressure in the ampule and potential rupture. It was also found that decafluorobiphenyl needed to be kept separate from the rest of the reactants in order for the crystals to grow. When decafluorobiphenyl was placed inside of the alumina crucible with the rest of the reactants, gray powder formed. Decafluorobiphenyl has a significantly lower melting point (67.5 °C) than the rest of the reactants; therefore, it is possible that upon melting, it readily reacts with one of the metals to make unreactive byproducts that terminate the reaction before the system can reach a high enough temperature to make a solution.

A wad of Fiberfrax was then placed above the alumina crucible to act as a filter when the reaction is complete. The silica sleeve was chilled in an ice bath for 5 min to lower the vapor pressure of $\rm C_{12}F_{10}$ before it was attached to the vacuum line for sealing. It was quickly flame-sealed under vacuum and placed in a programmable furnace. The ampule was heated to 950 °C in 3 h and held at 950 °C for 12 h. The reaction was then gradually cooled to 600 °C over the course of 120 h at which point it was taken out of the furnace, inverted, and placed into a centrifuge to remove the excess flux.

Elemental Analysis. Elemental analysis was performed on a FEI NOVA 400 scanning electron microscope equipped with energy-dispersive X-ray spectroscopy (SEM-EDS). Crystals of $La_{15}(FeC_6)_4F_2$ were mounted on an aluminum puck using double-sided carbon tape. To eliminate spurious readings from the flux residue on the surface, each crystal was cleaved and arranged on the carbon tape so that an inside surface is perpendicular to the electron beam. A 30 kV acceleration voltage was used for the EDS measurements. EDS confirmed the presence of lanthanum and iron. Carbon was not quantified due to the carbon tape background, and fluorine could not be reliably observed due to the overlap of the fluorine $K\alpha$ peak and the iron $L\alpha$ peak (at 0.677 and 0.705 eV, respectively). Quantifying only the metals, lanthanum and iron were found to be 78.3(3) and 21.7(3) at. %, respectively, which agrees well with the formula found from SC-XRD, $La_{14.7}(FeC_6)_4F_2$, which is 79.0 at. % La and 21.0 at. %

Structural Characterization—X-ray Diffraction. Suitable single crystals were collected and cut to size. The fragments were mounted onto cryoloops using paratone oil. SC-XRD data were collected at 296 K on a Rigaku XtaLAB Synergy-S diffractometer equipped with a HyPix-6000HE Hybrid Photon Counting detector and Mo/Cu microfocus-sealed X-ray sources. Mo Klpha radiation was used ($\lambda = 0.71073$ Å). The datasets were processed and integrated using the CrysalisPRO software. 14 The structure was refined using the Shelxle package. 15 Heavy atoms (La and Fe) were located using direct methods; carbon and fluorine positions were found by least-squares refinement and difference Fourier maps and assigned based on bond length considerations and comparison to the hydride analogue. Data collection parameters are shown in Table 1; additional data can be found in the crystallographic information file deposited with the Cambridge Crystallographic Data Centre under deposition number CSD 2212841.

Table 1. Crystallographic Parameters and Data Collection Information for ${\rm La_{14.7}(FeC_6)_4F_2}$

formula weight (g/mol)	2573.8
crystal system	hexagonal
space group	P6 (#174)
a (Å)	8.760(3)
c (Å)	10.720(4)
Z	1
volume (ų)	712.4
density, calc (g/cm ³)	6.00
index ranges	$-10 \le h \le 9$
	$-8 \le k \le 11$
	$-12 \le l \le 14$
reflections collected	2988
temperature (K)	296 K
radiation	Mo-K α (λ = 0.71073 nm)
unique data/parameters	1134/60
θ values (deg)	$\theta_{\min} = 1.900; \ \theta_{\max} = 29.938$
$\mu (\mathrm{mm}^{-1})$	23.3
$R_1/wR_2 (I > 2\sigma(I))$	0.0496/0.1180
R_1/wR_2 (all data)	0.0537/0.1203
flack parameter	0.6(3)
GoF	1.111
highest peak/hole (e-/ų)	6.00/-4.07

Several lanthanum sites in the structure are disordered, exhibiting site splitting and partial occupancies. As discussed in the next section, the occupancy of La5 is correlated with the occupancy of La2a (which is a split site with La2b). Upon free refinement, their occupancies refined to very similar values in the range of 73-76%. They were therefore constrained to be identical (75% occupied). The Flack parameter was refined to 0.6(3) to account for merohedral twinning. All La and Fe atoms were refined anisotropically. When the lighter atoms (F and C) were refined anisotropically, some of the thermal parameters became non-positive, so they were refined isotropically. However, large residual electron peaks were consistently observed along the c-axis below the fluorine site and above the associated La1 site (vide infra), indicating that both atoms are strongly anisotropic or exhibit site disorder. Attempts to add the q-peaks to the model led to refinement instability. To further explore this disorder and possible supercell formation, precession photos were taken in the -1kl and hk0 directions with an exposure time of 93 s. This fluorine site disorder and the partial occupancy of La sites are observed in all crystals that were examined.

■ RESULTS AND DISCUSSION

Synthesis. The title compound was chosen as a target to explore the viability of using an organic compound as a fluorine source in metal flux synthesis. This was inspired by our previous work using anthracene as a carbon and hydrogen source in metal flux synthesis, which yielded La₁₅(FeC₆)₄H.⁷ To investigate the incorporation of fluorine, decafluorobiphenyl $(C_{12}F_{10})$ was chosen as a carbon and a fluorine source. Upon heating, decafluorobiphenyl will decompose into gaseous species which dissolve in the flux and act as a source of carbon and fluorine. The formation of carbon is indicated by observation of a carbon film coating the inside of the ampule; dissolution of carbon in the La/Ni flux leads to formation of metal carbide products. The presence of fluorine is evidenced by the incorporation of fluoride interstitials in the product structure. La₁₅(FeC₆)₄F₂ forms as silver hexagonal rods up to 2 mm in length and 0.5 mm in diameter, see Figure 1. The compound can be handled in air briefly but decomposes after

2–3 h. In addition to the crystalline product, small amounts of unidentified powder byproduct are also formed.

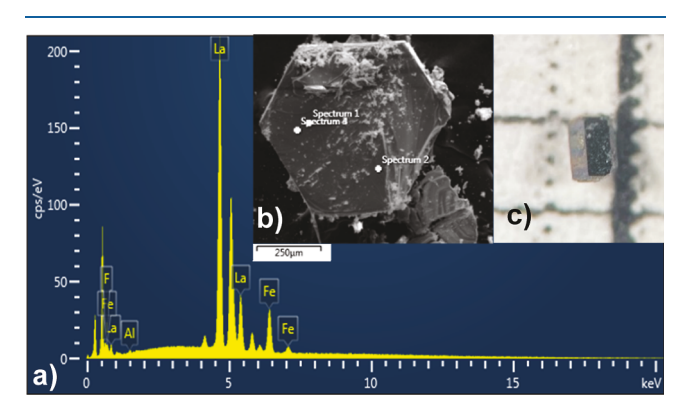


Figure 1. (a) SEM-EDS elemental analysis data for $La_{15}(FeC_6)_4F_2$. (b) SEM image of a single crystal. (c) Optical microscopy image of a crystal of $La_{15}(FeC_6)_4F_2$ on a millimeter grid paper.

Structure. The title compound crystallizes in the hexagonal crystal system with space group $P\overline{6}$; the structure is shown in Figure 2. It features tetrahedrally coordinated fluoride sites and FeC₆ units similar to those found in several carbometallates, including RE₁₅(FeC₆)₄H (RE = La and Pr), La_{3.67}FeC₆, and RE₁₅Fe₈C₂₅ (RE = Y, Dy, Ho, and Er). The FeC₆ unit is composed of a central iron atom bonded to three ethylene species. The Fe–C bond lengths range from 1.80(3) to 1.82(2) Å, and the C=C bond lengths range from 1.30(5) to 1.37(8) Å, in agreement with the previously cited literature. The three crystallographically unique FeC₆ units stack parallel to the c-axis; they are essentially trigonal planar with only slight variations from ideal 120° angles.

 $La_{15}(FeC_6)_4F_2$ and $La_{15}(FeC_6)_4H$ both form in the $P\overline{6}$ space group, with very similar unit cell parameters [a = 8.760(3) Å, c= 10.720(4) Å, and V = 712.4(5) Å³ for the fluoride and a = 10.720(4)8.7890(4) Å, c = 10.7691(5) Å, and V = 720.42(7) Å³ for the hydride]. Single-crystal neutron diffraction data were needed to verify the presence and half-occupancy of the hydride ions in the tetrahedral interstitial site (2g Wyckoff site) of La₁₅(FeC₆)₄H. This site lies across a mirror plane from its symmetry-equivalent; therefore, the two tetrahedral sites share a common triangular base. If a hydride is present in one tetrahedron, it is absent in its neighbor. For the La₁₅(FeC₆)₄F₂ compound studied here, the presence of fluoride on this 2g site was easily observable by SC-XRD. Unlike the hydride, this fluoride interstitial is fully occupied. Since both tetrahedra are occupied, the fluorine atoms shift further away from the common triangular base, as shown in Figure 3, resulting in a

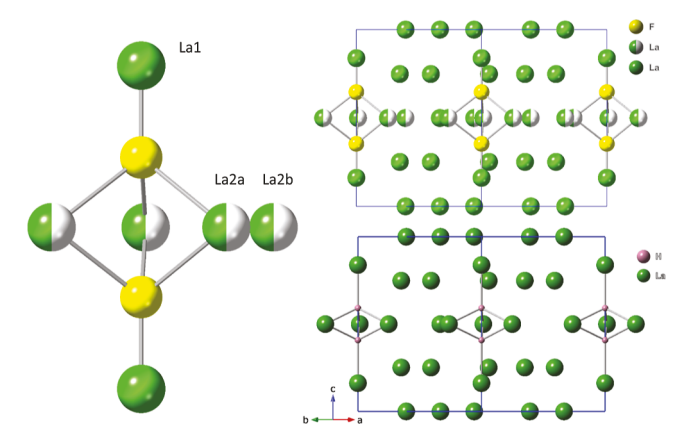


Figure 3. Local environment of the fluoride interstitial sites in $La_{15}(FeC_6)_4F_{2\nu}$ compared to the corresponding half-occupied hydride site in $La_{15}(FeC_6)_4H$. Unit cells viewed down the $\begin{bmatrix} 1 & 1 & 0 \end{bmatrix}$ direction. The FeC_6 units are omitted for clarity.

F–F distance of 3.32 Å. With the incorporation of fluorine, the surrounding lanthanum sites become partially occupied, with La1 being 90(2)% occupied and La2 becoming a split site with La2a being 76(1)% occupied and La2b being 24(1)% occupied. An additional La site (La5) that is coordinated by La2b also becomes partially occupied. These partial occupancies yield a stoichiometry of $La_{14.7}(FeC_6)_4F_2$. For simplicity, we are using the rounded stoichiometry $La_{15}(FeC_6)_4F_2$.

The lanthanide site splitting and partial occupancy are likely due to optimization of La–F bond lengths. Lanthanum—fluoride bond lengths are reported in the literature in compounds such as LaF₃ [with the F–La distances in LaF₃ ranging from 2.416(3) to 3.01(1) Å] and LaSnF₇ (La–F bond lengths ranging from 2.307 to 2.492 Å). ^{18,19} In La₁₅(FeC₆)₄F₂, the fluoride interstitial is 2.06(5) Å from La1, 2.77(3) Å from La2a, and 3.56(5) Å from La2b. The 2.06(5) Å distance to La1 is too short, which may induce both the partial occupancy of this La site and its strongly anisotropic thermal parameter along the *c*-axis. On the other hand, the 2.77(3) Å distance to the three surrounding La2a sites is within the range of expected F–La.

The X-ray data refinements of several crystals of the title phase consistently indicated two residual electron density peaks (Q1 and Q2) along the *c*-axis shown in Figure 4, likely caused by La1 and F trying to increase the distance from each other. This disorder is the probable cause for the splitting of the La2 site into La2a and La2b. As F moves closer to the mirror plane (to the Q1 site), the F-La1 distance would increase to 2.75 Å. However, this will decrease the F-La2a

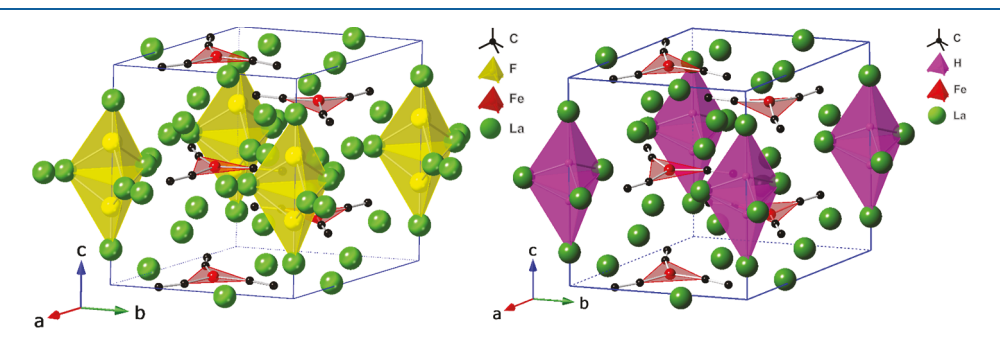


Figure 2. Structure of $La_{15}(FeC_6)_4F_2$, compared to that of $La_{15}(FeC_6)_4H$. Tetrahedral interstitial sites shown in a polyhedral mode.

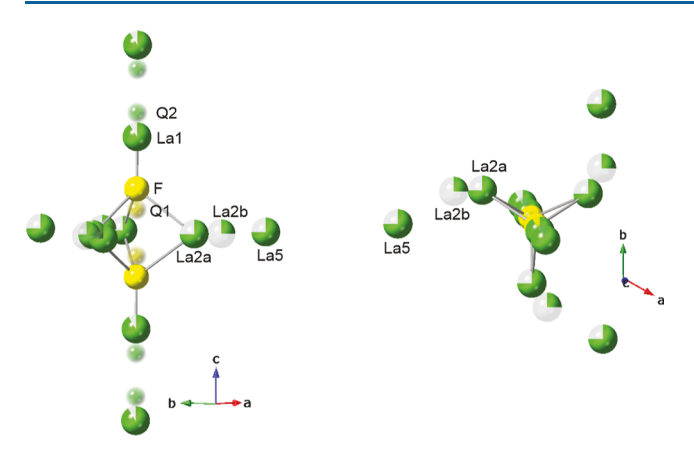


Figure 4. Disordered sites in $La_{15}(FeC_6)_4F_2$ showing the residual electron density peaks (Q1 and Q2) adjacent to the F and La1 positions, as well as the partial occupancy of surrounding La sites.

distance to 2.44 Å, causing La2a to move to the La2b positions. If the fluorine occupied the Q1 position entirely, the F–F distance across the mirror plane would be too short (1.76 Å). Conversely, if the La1 atom shifts away from the fluorine (to occupy the Q2 site), this yields a suitable F–La1 distance of 2.88 Å. However, it then becomes too close to the next La1 position along the c-axis (2.55 Å). Attempts to add the q-peaks to the model and define F/Q1 and La1/Q2 as split sites led to unstable refinements.

The La5 site is in the same *ab*-plane as the disordered La2a and La2b atoms and is trigonally coordinated by La2b with a La5—La2b distance of 2.39(1) Å. This is too short, so if La2b is occupied, La5 is unoccupied. This was apparent when the occupancy of La5 was allowed to freely refine; it refined to a value very similar to that of La2a. Therefore, the two feasible structures are Figure 5b (which has La2b occupied, and the other two are empty) occurring 25% of the time, and Figure 5c (which has La2a and La5 occupied, with La2b empty) occurring 75% of the time. The La2a to La5 distance is 3.37(5) Å. This disordering of the La sites occurs in all crystals examined.

This disordered La layer in the ab-plane containing multiple sites with partial occupancy (some of which are correlated) bears some resemblance to the disordered chain of La atoms in La_{3.67}FeC₆ reported by Witte and Jeitschko that was later found by Davaasuren et al. to form a supercell. ^{17,20} To explore this possibility, precession photos were taken to seek evidence of supercell formation (see Figure 6). Each zone photo had an exposure time of 93 s to enable detection of weak satellite peaks. The hk0 zone photo shows little evidence of supercell formation. However, streaking is visible in the -1kl direction owing to the disordered La layer in the ab-plane. Satellite peaks are also visible in the same direction, indicating that the structure may be trying to form a supercell; these peaks are not intense enough to allow for refinement of this cell.

CONCLUSIONS

The synthesis of $La_{15}(FeC_6)_4F_2$ was achieved by reacting iron and decafluorobiphenyl in excess La/Ni flux. This compound is a disordered variant of $La_{15}(FeC_6)_4H$, with fluorine fully occupying the interstitial hydride site as opposed to the half occupancy of H in the hydride structure. The full occupancy of the interstitial site by fluoride leads to disorder in the layer of adjacent lanthanum sites, with several La positions becoming

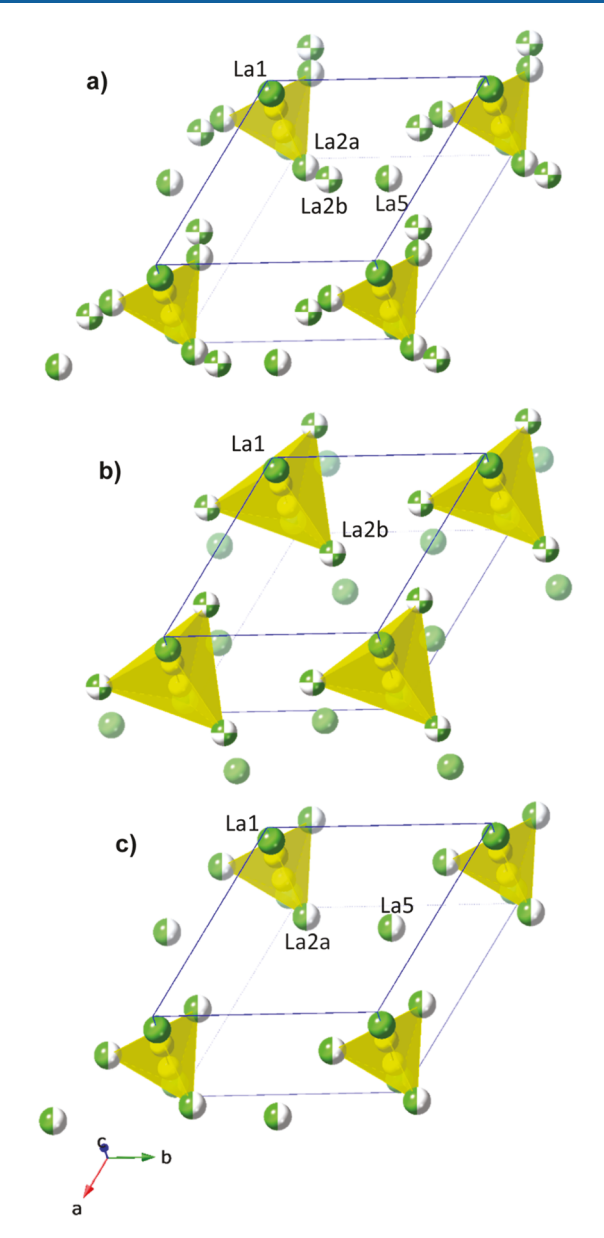


Figure 5. (a) Disordered La layer viewed down the c-axis. La3 and La4 are omitted for clarity. (b) One of the two possible structures with La2b being the only La atom present in the disordered layer. (c) Second possible structure, which has La2a and La5 present simultaneously.

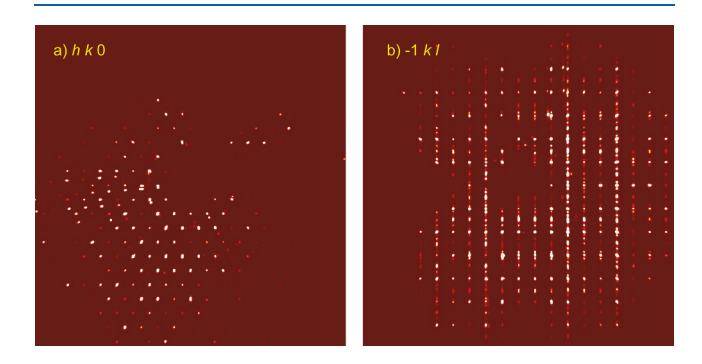


Figure 6. Precession photos of $La_{15}(FeC_6)_4F_2$. (a) hk0 photo. (b) -1kl photo which corresponds to the ab-plane. Streaking is visible due to the disorder in the La layer in that plane. Satellite peaks can also be seen, indicating the possibility of a supercell.

partially occupied and split, giving rise to two possible structures occurring in a ratio of approximately 75:25%. This introduces potential supercell formation, but the structure remains disordered. It is notable that the hydride interstitial in $\rm La_{15}(FeC_6)_4H$ does not induce similar disorder in the surrounding La sites. This may be due to the polarizability of the hydride anion which allows it to squeeze into the interstitial site, whereas the harder fluoride anion forces the surrounding La cations to adjust their positions. Variable-temperature diffraction studies are planned to see if this disorder induces a structure change at lower temperatures.

The synthesis of $La_{15}(FeC_6)_4F_2$ is notable because attempts to fluorinate metals or intermetallic phases typically lead to their decomposition into binary M_xF_y ionic compounds. This is due to the high reactivity of the strongly electronegative F^- anion.²² The inclusion of fluoride interstitials into an intermetallic rare-earth compound without decomposition is therefore striking, and this synthesis method may lead to new compounds with unusual electronic properties.

ASSOCIATED CONTENT

Accession Codes

CCDC 2212841 contains the supplementary crystallographic data for this paper. These data can be obtained free of charge via www.ccdc.cam.ac.uk/data_request/cif, or by emailing data_request@ccdc.cam.ac.uk, or by contacting The Cambridge Crystallographic Data Centre, 12 Union Road, Cambridge CB2 1EZ, UK; fax: +44 1223 336033.

AUTHOR INFORMATION

Corresponding Author

Susan E. Latturner — Department of Chemistry and Biochemistry, Florida State University, Tallahassee, Florida 32306, United States; orcid.org/0000-0002-6146-5333; Email: slatturner@fsu.edu

Author

James T. Larson – Department of Chemistry and Biochemistry, Florida State University, Tallahassee, Florida 32306, United States

Complete contact information is available at: https://pubs.acs.org/10.1021/acs.inorgchem.2c03642

Notes

The authors declare no competing financial interest.

ACKNOWLEDGMENTS

This research was supported by the Division of Materials Research of the National Science Foundation (DMR-18-08471 and DMR-21-26077). This work utilized the resources of the X-ray Characterization Center in the Department of Chemistry and Biochemistry at FSU (FSU075000XRAY). SEM equipment in the Biological Sciences Imaging Resource (BSIR) of the Florida State University Department of Biology was also used; we thank Dr. Eric Lochner for guidance with this instrument.

REFERENCES

(1) Kanatzidis, M. G.; Pöttgen, R.; Jeitschko, W. The Metal Flux: A Preparative Tool for the Exploration of Intermetallic Compounds. *Angew. Chem., Int. Ed.* **2005**, *44*, 6996–7023.

- (2) Latturner, S. E. Clusters, Assemble: Growth of Intermetallic Compounds from Metal Flux Reactions. *Acc. Chem. Res.* **2018**, *51*, 40–48
- (3) Phelan, W. A.; Menard, M. C.; Kangas, M. J.; McCandless, G. T.; Drake, B. L.; Chan, J. Y. Adventures in Crystal Growth: Synthesis and Characterization of Single Crystals of Complex Intermetallic Compounds. *Chem. Mater.* **2012**, *24*, 409–420.
- (4) Jayasinghe, A. S.; Latturner, S. E. Metal Flux Growth of Praseodymium Iron Carbides Featuring FeC3 Units. *Cryst. Growth Des.* **2021**, *21*, 103–111.
- (5) Engstrand, T. O.; Wei, K.; Baumbach, R.; Xin, Y.; Latturner, S. E. Structural Disorder in Intermetallic Boride Pr21M16Te6B30 (M = Mn, Fe): A Transition Metal Cluster and Its Evil Twin. *Inorg. Chem.* **2020**, *59*, 2484–2494.
- (6) Tucker, P. C.; Nyffeler, J.; Chen, B.; Ozarowski, A.; Stillwell, R.; Latturner, S. E. A Tale of Two Metals: New Cerium Iron Borocarbide Intermetallics Grown from Rare-Earth/Transition Metal Eutectic Fluxes. J. Am. Chem. Soc. 2012, 134, 12138–12148.
- (7) Engstrand, T. O.; Cope, E. M.; Vasquez, G.; Haddock, J. W.; Hertz, M. B.; Wang, X.; Latturner, S. E. Flux Synthesis of a Metal Carbide Hydride Using Anthracene As a Reactant. *Inorg. Chem.* **2020**, *59*, 11651–11657.
- (8) Hertz, M. B.; Baumbach, R.; Wang, X.; Latturner, S. E. Unexpected Hydride: Ce4B2C2H2.42, a Stuffed Variant of the Nd2BC Structure Type. *Cryst. Growth Des.* **2021**, *21*, 5164–5171.
- (9) Bowman, R. C.; Fultz, B. Metallic Hydrides I: Hydrogen Storage and Other Gas-Phase Applications. *MRS Bull.* 2002, *27*, 688–693. DOI: 10.1557/mrs2002.223; Cambridge University Press Cambridge Core From.
- (10) Miedema, A. R.; Buschow, K. H. J.; Van Mal, H. H. Which intermetallic compounds of transition metals form stable hydrides. *J. Less Common. Met.* **1976**, 49, 463–472.
- (11) Corbett, J. D.; Leon-Escamilla, E. A. Role of hydrogen in stabilizing new hydride phases or altering old ones. *J. Alloys Compd.* **2003**, 356–357, 59–64.
- (12) Leon-Escamilla, E. A.; Corbett, J. D. Compounds of alkalineearth and divalent rare-earth metals stabilized by hydrogen impurities. The Yb5Sb3 and Mn5Si3 structure types for pnictides. *J. Alloys Compd.* 1994, 206, L15–L17.
- (13) Henning, R. W.; Leon-Escamilla, E. A.; Zhao, J.-T.; Corbett, J. D. Stabilization by Hydrogen. Synthetic and Structural Studies of the Zintl Phase Ba5Ga6H2. *Inorg. Chem.* **1997**, *36*, 1282–1285.
- (14) CrysAlisPRO; Oxford Diffraction; Agilent Technologies UK Ltd: Yarnton, England.
- (15) Hübschle, C. B.; Sheldrick, G. M.; Dittrich, B. ShelXle: a Qt graphical user interface for SHELXL. *J. Appl. Crystallogr.* **2011**, 44, 1281–1284.
- (16) Davaasuren, B.; Borrmann, H.; Dashjav, E.; Kreiner, G.; Widom, M.; Schnelle, W.; Wagner, F. R.; Kniep, R. Planar Fe6 Cluster Units in the Crystal Structure of RE15Fe8C25 (RE=Y, Dy, Ho, Er). *Angew. Chem., Int. Ed.* **2010**, 49, 5688–5692.
- (17) Witte, A. M.; Jeitschko, W. Preparation and Crystal Structure of the Isotypic Carbides Ln3.67TC6 (Ln = rare earth elements; T = Mn, Fe, Ru) and Eu3,16NiC6. Z. Naturforsch. B 1996, S1, 249–256.
- (18) Zalkin, A.; Templeton, D. H.; Hopkins, T. E. The Atomic Parameters in the Lanthanum Trifluoride Structure. *Inorg. Chem.* **1966**, *5*, 1466–1468.
- (19) Graudejus, O.; Müller, B. G. Neue Fluoride MIIIMIVF7 mit MIII = SE, Tl und MIV = Sn, Pb, Pt. Z. Anorg. Allg. Chem. 1996, 622, 1601–1608
- (20) Davaasuren, B.; Dashjav, E.; Kreiner, G.; Borrmann, H.; Kniep, R. Reinvestigation and superstructure of La3.67[Fe(C2)3]. *J. Solid State Chem.* **2009**, *182*, 1331–1335.
- (21) Messer, C. E. Hydrides versus fluorides: Structural comparisons. *J. Solid State Chem.* **1970**, *2*, 144–155.
- (22) Vaney, J.-B.; Vignolle, B.; Demourgues, A.; Gaudin, E.; Durand, E.; Labrugère, C.; Bernardini, F.; Cano, A.; Tencé, S. Topotactic fluorination of intermetallics as an efficient route towards quantum materials. *Nat. Commun.* **2022**, *13*, 1462.